THE LATEST BATHYMETRY AND TOPOGRAPHY EXTRACTION OF LAKE LEDULU FROM MULTI-SOURCE GEOSPATIAL DATA

Atriyon JULZARIKA [1, 2*], ***Dany Puguh LAKSONO*** [3, 4], ***Luki SUBEHI*** [5], ***Elisa ISWANDONO*** [6], ***Alfred Onisimus Maximus DIMA*** [7], ***Media Fitri Isma NUGRAHA*** [8], ***Kayat KAYAT*** [9]

DOI: 10.21163/GT_2023.182.14

ABSTRACT:
Topography is the basic geospatial information that is used as the main reference in the extraction of thematic geospatial information. It consists of terrestrial topography (topography) and underwater topography (bathymetry). One of the problems related to topography is the availability of detailed and up-to-date topographic and bathymetry data. This research proposes the latest bathymetry and topography extraction modeling with multi-source geospatial data including PlanetScope, Sentinel-1, Landsat images, and in-situ field data. The study area is located in Lake Ledulu, Rote Island, Indonesia. Bathymetry and topography were extracted using PlanetScope imagery and in-situ field data using the least squares adjustment computation approach. The mathematical design model uses the latest DTM method, which correlated with in-situ data. Time-series Landsat and PlanetScope are used to extract the lake bank boundaries with water using the harmonic method. DEM integration method is used to integrate bathymetry and topography. The updated topography and bathymetry are performed by adding the true vertical deformation extracted from Sentinel-1 imagery using the D-InSAR method. The results obtained are the latest bathymetry and topography of Lake Ledulu in 2022 or so-called DTM $_{(2022)}$. Then DTM $_{(2022)}$ is tested for profile checking and vertical accuracy at the confidence level of 95 % according to the ASPRS 2014. The DTM $_{(2022)}$ of Lake Ledulu has a vertical accuracy of $\pm$ 61.54 cm or according to 1:5000 – 1:10000 scale mapping. DTM $_{(2022)}$ is also used to determine the dynamics of the volume of Lake Ledulu and its changes from 1985 to 2022. In 2022 (dry season) Lake Ledulu has a surface area (0.0946 km^2), volume (701,688.45 m^3), and perimeter (1.868 km). In 2022 (wet season), Lake Ledulu has a surface area (0.1555 km^2), volume (1,116,525.9 m^3), and perimeter (2.612 km). In 1985 (wet season) Lake Ledulu have surface area (0.3079 km^2), volume (4,772,567.2 m^3), and perimeter (3.477 km). The change in the surface area of Lake Ledulu from 1985-2022 was 0.1525 km^2 (decrease of 49.53%). The volume of Lake Ledulu from 1985-2022 was 3,656,041.3 m^3 (decrease of 75.61%). Change in the perimeter of Lake Ledulu 1985-2022 was 0.862 km (shrinkage of 24.79%).

Key-words: *Bathymetry, Topography, Lake Ledulu, Dynamics Volume, Multi-Source Geospatial Data*

[1] *Research Center for Geospatial-BRIN, Cibinong, Indonesia, atri001@brin.go.id ; verbhakov@yahoo.com*
[2] *Department of Earth Technology, Gadjah Mada University, Yogyakarta, Indonesia, atriyonjulzarika@mail.ugm.ac.id*
[3] *Department of Geodetic Engineering, Gadjah Mada University, Yogyakarta, Indonesia, danylaksono@ugm.ac.id*
[4] *Department of Computer Science, City, University of London, dany.laksono@city.ac.uk*
[5] *Research Center for Limnology and Water Resources, Cibinong, Indonesia, luki001@brin.go.id*
[6] *Natural Resources Conservation Center of East Nusa Tenggara, Ministry for Environment and Forestry (KLHK), Kupang, Indonesia, eiswandono@gmail.com*
[7] *Department of Biology, Nusa Cendana University, Kupang, Indonesia, dimaonny@gmail.com*
[8] *Research Center for Pharmaceutical Ingredients and Traditional Medicine-BRIN, Cibinong, Indonesia, medi005@brin.go.id*
[9] *Research Center for Applied Zoology-BRIN, Kupang, Indonesia, kaya001@brin.go.id*
** Corresponding author's email: atri001@brin.go.id and verbhakov@yahoo.com*

1. INTRODUCTION

Topographic mapping technology is one of the geospatial technology which has developed rapidly (Wilson, 2012). Topography is the basic geospatial information that is used as the main reference in the extraction of thematic geospatial information (Julzarika & Harintaka, 2020). Topography study of the shape of the Earth's surface and other objects, including planets, natural satellites, and asteroids (Jenson & Domingue, 1988). In general, topography studies surface relief, 3-dimensional models, and the identification of land types (Julzarika & Djurdjani, 2018). Topography consists of terrestrial topography (topography) and underwater topography (bathymetry). The underwater topography is often referred to as bathymetry (Inglada & Garello, 2002). Bathymetry is divided into two types, namely seawater (marine) bathymetry, and inland water bathymetry (Julzarika et al., 2021). Seawater bathymetry uses a height reference field which refers to the lowest ebb in 1 tidal period (18.61 years) (IHB, 2006). Inland water bathymetry uses a height reference field regarding the highest tide (Julzarika et al., 2021). Inland water includes lakes, rivers, and reservoirs. Topographic data can be obtained by terrestrial surveys or by non-terrestrial surveys (Julzarika & Djurdjani, 2018). Terrestrial survey is carried out by direct measurements in the field using surveying tools such as a theodolite, leveling, total station, and terrestrial laser scanner (TLS) (Julzarika & Harintaka, 2019; Suhadha & Julzarika, 2022). Non-terrestrial surveys are carried out by mapping with satellites, planes, air balloons, Unmanned Aerial Vehicles (UAV), and Unmanned Surface Vehicles (USV) (Julzarika & Djurdjani, 2018; Suhadha & Julzarika, 2022). The results of measurements with terrestrial surveys and with non-terrestrial surveys are often presented as 3D visualization data (Fukuda et al., 2016; Nasir et al., 2015). The result of the data modeling and visualization is Digital Terrain Model (DTM). DTM is topographic or terrain modeling (bare earth) without any natural objects or features such as vegetation, buildings, and other artificial objects (Li et al., 2004). DTM can be used to predict past and future topography.

Currently, the availability of detailed terrain and underwater topographic data is a major problem in many countries (Julzarika, Aditya, Subaryono, & Harintaka, 2021). Not only detailed topographical data are mostly unavailable, but lack of up-to-date topography is also an important problem in many countries. The availability of underwater topography (bathymetry) is also a major constraint for mapping in various countries (Alpers & Hennings, 1984; Pleskachevsky et al., 2011). These detailed DTM updates can be made with the latest DTM products (Julzarika, 2021). The main problem with detailed topographic mapping and bathymetry in most countries is the expensive cost of mapping, as well as it is time consuming (Ruzgiene et al., 2015; Samboko et al., 2020; Uysal et al., 2015). The latest DTM can be an alternative solution for detailed topographic mapping and bathymetry at a low cost.

The latest DTM is a terrain and underwater topographic model with the latest conditions obtained from the integration of the DTM master with the up-to-date vertical deformation (Julzarika, Aditya, Subaryono, & Harintaka, 2021). The DTM includes topography and bathymetry (underwater topography). DTM master can be extracted by certain methods based on the type of input data (Julzarika, 2021). The input data are optical data, SAR data, microwave data, sonar data, or Light Detection and Ranging (LiDAR) data. The optical data that can be used to extract bathymetry and topography are PlanetScope, WorldView, Pleiades, etc. The SAR data that can be used to extract topography are ALOS-2, TerraSAR X, Radarsat, etc. The output of the processing of the input data is Digital Surface Model (DSM) and DTM (bathymetry and topography). The methods used to extract topography are reverse stereo, stereo model, triplet model, multiview model, and videogrammetry (Bignone et al., 2008; Julzarika & Djurdjani, 2018). The method used for Synthetic Aperture Radar (SAR), microwave, and sonar data is interferometry (Costantini, 1998; Julzarika, Aditya, Subaryono, & Harintaka, 2021; Nico et al., 2005; Rucci et al., 2012; Simons & Rosen, 2015). DTM master is obtained after the conversion of DSM to DTM.

Studies related to bathymetric extraction have been carried out. Bathymetric extraction with PlanetScope imagery in the Kemujan Island area using the Stumpf algorithm on the in-situ depth data (Sesama et al., 2021). In addition, there is also a bathymetric extraction using SPOT 7 images using the Random Forest method (Setiawan et al., 2019). The Satellite Derived Bathymetry (SDB)

method used in empirical bathymetry modeling on PlanetScope satellite imagery uses the Band Ratio algorithm in the Shallow Sea waters of Karimunjawa Island (Hambali et al., 2021). Bathymetry extraction can also be performed by correlating PlanetScope and Landsat images. In addition, research related to PlanetScope image bands is more representative of bathymetric extraction. The results of this study are linear regression which is more representative than SVR-based modeling, with the best single band modeling from the (ln) Green band and the best band ratio modeling from the ratio transformation of (ln) Blue/(ln) Green (Wulandari & Wicaksono, 2021). This paper will discuss the latest bathymetry and topography extraction modeling with multi-source geospatial data including PlanetScope, Sentinel-1, Landsat images, and in-situ field data. The novelty of this research is the bathymetry and topography modeling method of Lake Ledulu on Rote Island. This study aims to model the bathymetry and topography of Lake Ledulu with multi-source geospatial data (PlanetScope, Sentinel-1, Landsat, and in-situ data).

2. STUDY AREA

This study was carried out in Lake Ledulu, Rote Island, as can be seen in **figure 1**. Lake Ledulu is located in Rote Ndao Regency, East Nusa Tenggara Province, Indonesia. Based on the results of geo-forensics and geomodelling of the Expedition *Oe* 2017-2022, Lake Ledulu was formerly located on East Rote Island. *Oe* means water in the traditional Rote language. East Rote Island is located in the northern part of Rote Island. West Rote Island is similar to Southern Rote and East Rote Island is similar to Northern Rote. Administratively, Lake Ledulu is currently located in Landu Leko, Rote Ndao Regency (Ndao, 2021). Rote is the foremost island of Indonesia and a semi-arid area, located in the southern part area (Julzarika, et al., 2018; Ndao, 2021). There are 96 islands in Rote Ndao Regency, but only six islands are inhabited (Julzarika, et al., 2018). Rote Island is the largest island in this area and was formed from the combination of the Western Rote Island with the Eastern Rote Island at the end of the 19th century. East Rote Island is known as the Rote Dead Sea Area or previously the *Matara Maka* area (Julzarika et al., 2020). Matara Maka was the first inhabitant of this island who came from Australia. The Matara tribe is one of the lost aboriginal tribes in Northern Australia and had completely moved to Rote Island, Timor Island, South Papua, and southern Maluku. They migrated by following the *Makassarese* shipping route from Northern Australia (Kampung Jawa and Marege) to Makassar. The merger of West Rote Island with East Rote Island was caused by high vertical deformation in this area (Julzarika et al., 2021). Rote Ndao itself was formed from the Indo-Australian plate which was separated from the Australian continent due to the subduction of the Eurasian plate (Hall, 2011; Malaspinas et al., 2016; Suhadha & Julzarika, 2020).

The result of Expedition *Oe* 2017-2022 describes that the geological conditions in Rote have similarities with Australia (Julzarika, et al., 2018; Laksono et al., 2019). As an example, mud volcanoes were found at several points, especially in the confluence area of West Rote Island with East Rote Island. In addition, there are 82 lakes, 24 of which are saltwater lakes found in Rote Ndao (Julzarika, et al., 2018). The salinity of these 24 saltwater lakes are between 26 and more than 100 ppt with high contents of Kalium, Natrium, and Magnesium of the stones around the lakes. In saltwater lakes, we found seawater and freshwater flora-fauna living together. Furthermore, some of the flora and fauna in Rote are endemic such as Rote Turtle (*Chelodina Mccordi*), Rote lizard, Matara fish, Ledulu fish, Rote bird (*Myzomela irianawidodoae*), and Tunjung flower (Julzarika et al., 2018). On the mainland, many mangroves are found on the top of hills and far from the waters.

Lake Ledulu in Rote language means the Easternmost Lake. Lake Ledulu is a tectonic lake formed due to non-uniform uplift around East Rote. The sub-fault that forms Lake Ledulu extends from north to south. The high uplift on the west and east sides of the sub-fault forms high cliffs (50-200 m). Non-uniform uplift occurs along fault lines. As a result, freshwater pools form from rainwater sources. There are 3 sources of fresh water in Lake Ledulu, located in the northern part of the lake. The rocks in Lake Ledulu are sea corals that are uplifted with marine vegetation and fauna ecosystems. There are still many fossils of seashells and mangroves that grow around the lake and on the cliffs far from water sources. The rocks of Ledulu Lake have very high salinity, but the lake water is still relatively fresh.

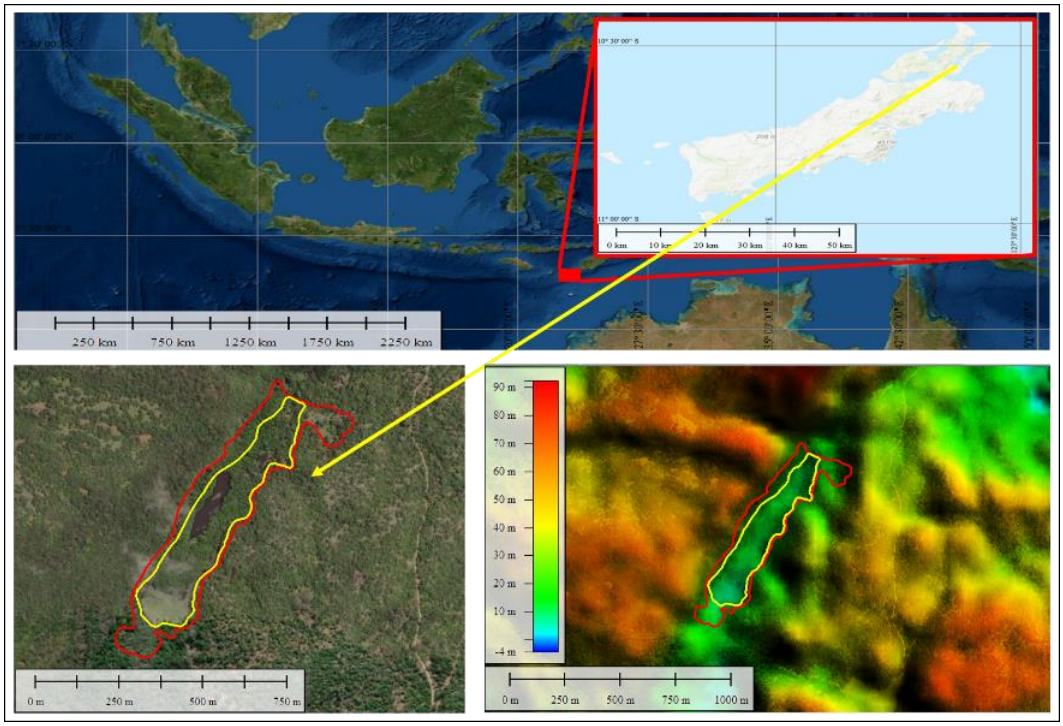

A

B

C

Fig. 1. A - 3D view of Lake Ledulu, located on Rote Island, Indonesia.; **B -** The fault passes through the northern part of Lake Ledulu, which is marked by steep cliffs.; **C -** The field view of Lake Ledulu.

The vegetation in Lake Ledulu and its surroundings is a mixture of terrestrial vegetation and coastal vegetation. Around the 1400s, Lake Ledulu was still a sea. At that time, it was still small islands and not yet connected as it is now, as this area was still uninhabited. Then around the 1700s, the East Rote area, where Lake Ledulu is located, became an inhabited island due to the arrival of groups of Aborigines from Australia. This sub-ethnic group that came from the Matara, a semi-arid area of the Northern Australia. The name of their leader was *Matara Maka* and made this eastern island of Rote the *Matara Maka* area. At the time of the group's arrival, the snake-necked turtles were also removed, making them an endemic species to Rote Island. All of this information was obtained from interviews with the Matara family around Lake Ledulu. Until now, Lake Ledulu and other lakes around it still belong to the Matara tribe. The East Rote area, like Lake Ledulu, has many snakes, Rote lizards, and other reptiles/amphibians that are unique and endemic.

3. DATA AND METHODS

3.1. Data

The data used are PlanetScope, Sentinel-1, Landsat, and in-situ data (bathymetry and topography measurement). PlanetScope imagery is an optical satellite belonging to the Planet company which consists of many satellites with a spatial resolution of 3 m. The details are 88 Dove satellites (February 2017) and an additional 48 Dove satellites (July 2017). The advantage of the PlanetScope satellite is that it can make acquisitions every day with 4 spectral bands (blue, green, red, NIR). In August 2021, Planet updated the satellite's original dove with the next generation of Doves. All PlanetScope images can still be acquired daily with 8 spectral bands (blue, green, red, NIR, green I, red edge, yellow, and coastal blue). NIR, blue, and coastal blue bands can be used for bathymetry extraction. The optimal red edge band is used for vegetation applications, and yellow is used for rock, soil, and mining applications. All PlanetScope bands can be utilized for extraction of DSM, DTM, vegetation height, canopies, buildings, and bathymetry. PlanetScope has derivative products in the form of PS2, PS2.SD, and PSB.SD.

Sentinel-1 is a C-band SAR satellite owned by European Space Agency (ESA) and Copernicus. Sentinel-1 is part of creating a radar observatory in Europe. The Sentinel-1 mission includes C-band imaging, operating in four proprietary imaging modes with different resolutions (up to 5 m) and ranges (up to 400 km). These conditions provide dual polarization capabilities. Sentinel-1 has a radial recording pattern making it optimal for vertical deformation applications. Sentinel-1 consists of Sentinel-1a and Sentinel-1b, each of which has a temporal resolution of 12 days. If used simultaneously, Sentinel-1 data can be obtained every 7-8 days.

Landsat is earth observation satellites for natural resources that uses optical sensors. This satellite has had 9 generations and was first launched in 1972. Landsat is owned by the United States of Geological Survey (USGS), and all data can be accessed free of charge from the USGS web. There are optical sensors on Landsat such as Coastal blue, Blue, Green, Red, NIR, SWIR, Thermal, Cirrus, and Panchromatic. Landsat spatial resolution for multispectral sensors is 30 m and 15 m spatial resolution for panchromatic sensors. Landsat and PlanetScope are optical satellites and complement each other in this research.

3.2. Methods

Bathymetry and Topography Extraction

Bathymetry and Topography are extracted with the Latest DTM method which displays the up-to-date conditions according to the conditions of the input data. This method uses the integration of the DTM master with vertical deformation (true). The input data used for bathymetry and topography are PlanetScope and vertical deformation (true) using Sentinel-1. Eq. 1 and eq. 2 is the latest DTM algorithm (Julzarika, 2021; Julzarika, Aditya, Subaryono, & Harintaka, 2021).

$$\text{The latest DTM} = \text{DTM master} \pm \text{the latest vertical deformation (true)} \quad (1)$$

$$\text{DTM master} = \text{DSM} + \text{height error correction} + \text{geoid undulation} \quad (2)$$

where DSM is extracted by InSAR (topography using SAR), reverse stereo (single optical images), LiSAR (SAR bathymetry), or SDB (optical bathymetry). Height error correction includes vegetation height, radius, and angle of view to the top of the surface object. Geoid undulation refers to the height reference field of Earth Gravitational Model (EGM) 2008.

The D-InSAR method is used to obtain vertical deformation information (uplift and subsidence) (Devanthéry et al., 2016; Herrera et al., 2013; Julzarika et al., 2022; Rucci et al., 2012; Simons & Rosen, 2015). The results of SAR extraction with D-InSAR are still in the form of vertical displacement-Light of Sight (LoS) which are the results of SAR extraction with D-InSAR. LoS correction to true is needed to convert vertical displacement (LoS) into vertical deformation (true) using equation 3 (Julzarika, 2021; Suhadha et al., 2021).

$$\text{The latest vertical deformation (true)} = \text{vertical displacement (LoS)} / \text{Cos}(\theta) \quad (3)$$

where θ is the incidence angle of SAR images

SDB is an alternative method that can replace Single-Beam Echo Sounder (SBES), Multi-Beam Echosounder (MBES), and Airborne Lidar Bathymetry (ALB) for measuring depth. This method is generally applied to relatively shallow waters. The measurement results of this method are also able to provide good correlation and accuracy values. The application of SDB requires satellite imagery as its dataset is complemented by in situ depth data. In this study, to get the SDB, the calculation is done by the least squares adjustment computation. This condition is caused by the number of measurements being greater than the number of parameters. Each pixel in satellite imagery can be predicted for its depth value after obtaining the values parameter of the design transformation model for the field measurement matrix (X). Equation (4) is a calculation of SDB by the least squares adjustment computation.

$$X = -(A^T PA)^{-1} A^T PF \quad (4)$$

X = matrix parameter transformation matrix A to matrix F.
A = design matrix of bathymetry and topography model.
F = ground measurement of bathymetry and topography matrix or approach measurement (comparison)
P = Weight matrix (using variant-covariant of bathymetry and topography from the sensor, ground, and model.

The DTM (bathymetry and topography) needs to be tested for vertical accuracy assessment. It includes the height difference test (equation 5) and the vertical accuracy test (equation 6 and 7). The height difference test aims to determine the vertical accuracy value at a certain tolerance so that it can be used to eliminate systematic errors that still exist in the height model (Julzarika, 2015). The height difference test can be useful in determining the height difference between two or more points. The method is to check at least 25 points on an area of 500 km^2 with a 95% confidence level (1.96 σ). The vertical accuracy test refers to the ASPRS 2014 standard (ASPRS, 2014).

$$\text{Height different test} = \Sigma (H_{n1} - H_{n0}) \quad (5)$$

where H_{n1} = the next height point in the polygon; H_{n0} = the before height point in the polygon

$$\text{Vertical accuracy test} = 1.96 * \text{RMSE}(z) \quad (6)$$

$$\text{RMSE}(z) = [(\Sigma(H_{data} - H_{check})^2/n)^{1/2}] \quad (7)$$

where H = orthometric height; n = sum of height point (minimum 25 height points in a project area (500 km^2); RMSE(z)=Root Mean Square Error for Vertical

If the bathymetry and topography meet the specified standards, a cross and longitudinal profile check is carried out. Subsequently, it can be used for various mapping applications such as contour extraction, vegetation height, land subsidence, and uplift.

Integration of Bathymetry (Lake) with Topography

DEM integration is combining data by involving two or more sets of data. The combination considers cofactor values and covariance variance between data (Julzarika et al., 2021). DEM integration is a method of integrating high data and/or n-dimensional data with weighting on each data based on the covariance variance calculated by least square adjustment computation (Hoja & D'Angelo, 2010; Julzarika et al., 2021). The calculation uses the smoothing method, where the number of measurements is more than the number of parameters (Ghilani & Wolf, 2006; Z. Li et al.,

2005). The determination of the boundary of the lake is done by using the harmonic method approach (Julzarika, et al., 2019). This harmonic method is a tidal observation (inland water with the highest tide) using time series data every month (Julzarika & Harintaka, 2020). The detailed explanation regarding this harmonic method refers to Julzarika, et al., (2019).

The harmonic method is used to extract the lake bank boundaries with water. The input data used is time-series satellite imagery. The results of determining the edge of a lake or beach will be optimal if using satellite imagery for 18-19 years. This condition is similar to tidal observations for 1 period in determining the coastline. Calculations using the Harmonic method are based on a least square adjustment computation. The shoreline of the lake from 1972-2022 was monitored also using time-series Landsat images.

Calculation of surface area and volume of lakes

The surface area of the lake is calculated based on the results of the extraction of the lake's edge boundaries. Lake volume calculation using the volume formula with the cut-and-fill method (Baek & Choi, 2017; Kubla, 2019). Cut-and-fill method is a soil or ice surface work process in which several materials, both soil, ice surface, or rocks, are taken from a certain place and then moved to another place to create the desired elevation. The bottom of the layer (elevation in bathymetry and topography) act as a zero-reference plane and is used to calculate the volume based on the cut-and-fill method. The grid method is used in the volume calculation (Kubla, 2019). The volume calculation based on the cut-and-fill method is easier due to the elevation and height differences being known based on the zero-reference plane. The grid method describes a uniform grid on each soil surface that is cut and filled. Each grid will have a different elevation according to the cut and fill sections (Julzarika, 2015). The total cut and fill volume is obtained by adding each pixel together. The volume of each pixel is obtained by multiplying the depth by the pixel area or the project area (Kubla, 2019).

4. RESULTS AND DISCUSSIONS

Discussion regarding the results includes bathymetry (wet season and dry season), vertical deformation, vertical accuracy tests, and the application of the DTM $_{(2022)}$ to predict past topographical conditions and future predictions. We extract the underwater topography (bathymetry) of Lake Ledulu based on the season conditions (wet and dry seasons). The height reference field of the inland water is the highest water level. The difference in the water level of the two seasons has a significant effect on the determination of the surface area and volume. Vertical deformation is also a major influence in determining the bathymetry and topography used. High uplift events affect the rise in the bottom of the lake and cause a change in its depth.

4.1. Bathymetry and topography of Lake Ledulu in dry season 2022

The dry season referred to in this study is the dry season that occurs on Rote Island. Rote Island is a semi-arid area. The dry season occurs from March to November. The peak of summer occurs in October-November which is characterized by hot temperatures ($> 40^0$ C) with strong winds, general drought throughout the region, and very rare rain. **Figure 2** is a display of the surface area of Lake Ledulu in the dry season. The water leveling that occurs in Lake Ledulu during the dry season has a elevation 0.5-3 m lower" to the water level during the wet season. Based on field measurements, in 2022 the water level difference was 0.9 m between the dry season and the wet season. In 2018-2020 (before the Seroja storm), the Rote Island area experienced maximum drought, with many droughts occuring in small lakes. Medium and large lakes experienced reductions in volume. Lake Ledulu is a medium-sized lake. After June 2020 (after the Seroja storm), there was a change in rainfall and the lake water level became higher than before the storm. One of the affected lakes is Lake Ledulu. In 2022 (wet season) Lake Ledulu had a surface area of 0.0946 km^2 and a volume of 701,688.45 m^3. The total length/perimeter of Lake Ledulu was 1.868 km.

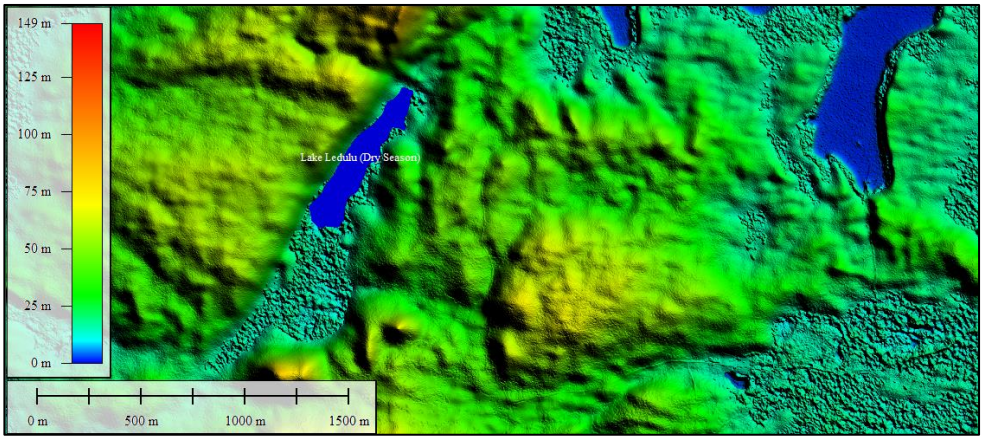

Fig. 2. Bathymetry and topography of Lake Ledulu in the dry season (2022)

4.2. Bathymetry and topography of Lake Ledulu in wet season 2022

The rainy season or wet season only occurs for 3 months on Rote Island, with the peak of the highest rainfall occurring in December. During this rainy season, the addition of water level in Lake Ledulu is 2 to 3 m. This has an impact on increasing the surface area, volume, and circumference of the lake. The surface area of Lake Ledulu in the wet season was 0.1555 km^2 with a volume of 1,116,525.9 m^3. The total perimeter was 2.612 km. Based on these values, there is a significant addition to Lake Ledulu from the dry season to the wet season. The addition of the surface area of Lake Ledulu was 60.83%. The addition of lake volume was 62.85%. The lake perimeter addition was 71.52%. **Figure 3** is the display of bathymetry and topography in the wet season (2022).

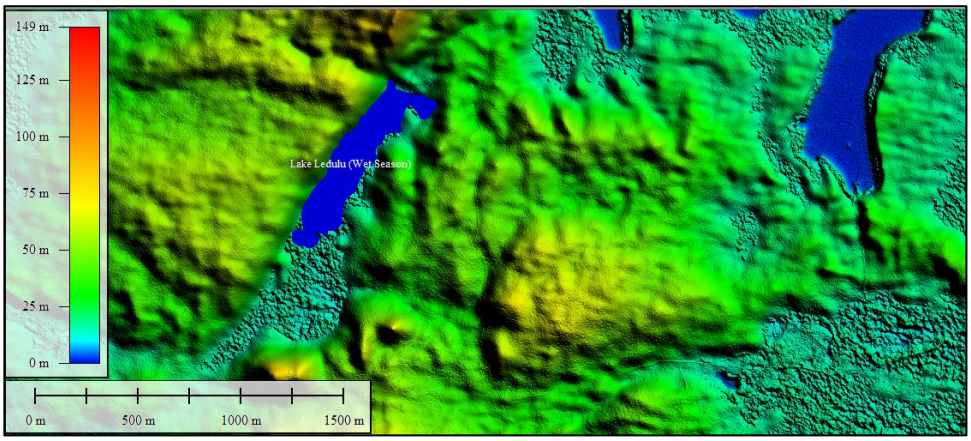

Fig. 3. Bathymetry and topography of Lake Ledulu in the wet season (2022).

4.3. Bathymetry and topography of Lake Ledulu in wet season 1985

Lake Ledulu's variations from 1985 to 2022 were carried out to establish changes in Lake Ledulu over the past 37 years. The surface area in the wet season of 1985 was used. In 1985, the surface area and volume of Lake Ledulu were still large. The dominant vertical deformation in Rote affected the reduction of the surface area and volume of Lake Ledulu. We can compare it with our last research on Rote Island. Based on measurement data from the expedition *Oe* 2017-2022, Rote Island experienced an uplift in the range of 13-25 cm/year (Julzarika et al., 2018). In this study, the uplift value in Rote was 13 cm/year. **Figure 4** is the bathymetry and topography of Lake Ledulu in the wet season (1985).

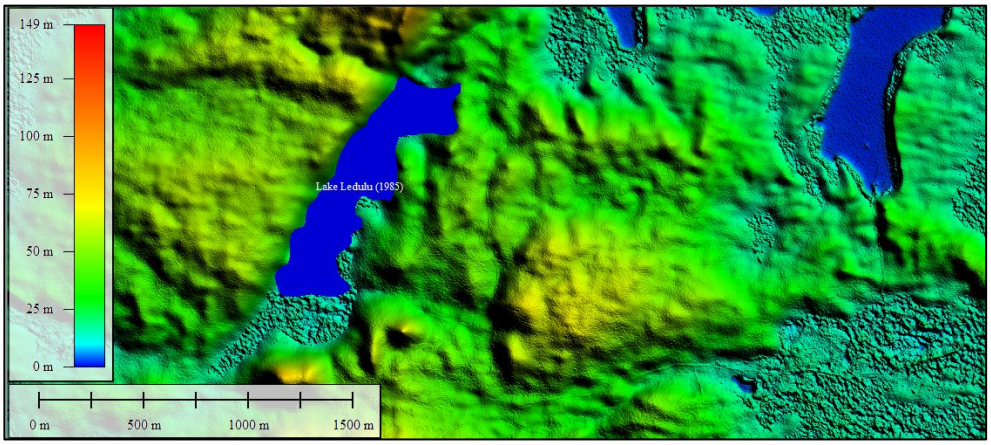

Fig. 4. Bathymetry and topography of Lake Ledulu in the wet season (1985).

DTM results (1985) can be compared in harmonic modeling and visually with Landsat imagery 1972-1985 to determine the shape of the lake shoreline. These conditions were used to extract the fixed boundaries of the shores of Lake Ledulu in that period. The fixed boundary on the shores of Lake Ledulu used is during the wet season. The surface area of Lake Ledulu in 1985 was 0.3079 km^2 with a perimeter of 3.477 km. Based on bathymetry data (2022), vertical deformation (1985-2022), and surface area of Lake Ledulu (1985), the volume can be calculated. The volume of Lake Ledulu was 4,772,567.2 m^3. Changes in surface area and volume of Lake Ledulu (1985-2022) can be calculated based on previously available geospatial information. Changes are calculated based on the wet season.

The change in the surface area of Lake Ledulu from 1985-2022 was 0.1525 km^2. Changes in the surface area of Lake Ledulu experienced a decrease of 49.53%. The volume of Lake Ledulu 1985-2022 was 3,656,041.3 m^3. Changes in the volume of Lake Ledulu experienced a decrease of 75.61%. Changes in the perimeter of Lake Ledulu 1985-2022, namely 0.862 km. Changes in the perimeter of Lake Ledulu experienced a shrinkage of 24.79%. The shrinkage of lake volume, lake surface area, and perimeter of the lake is caused by the dynamics of the seasons, the amount of rainfall, and the dynamics of vertical deformation. **Figure 5** is the display of the bathymetry and topography of Lake Ledulu (1985-2022).

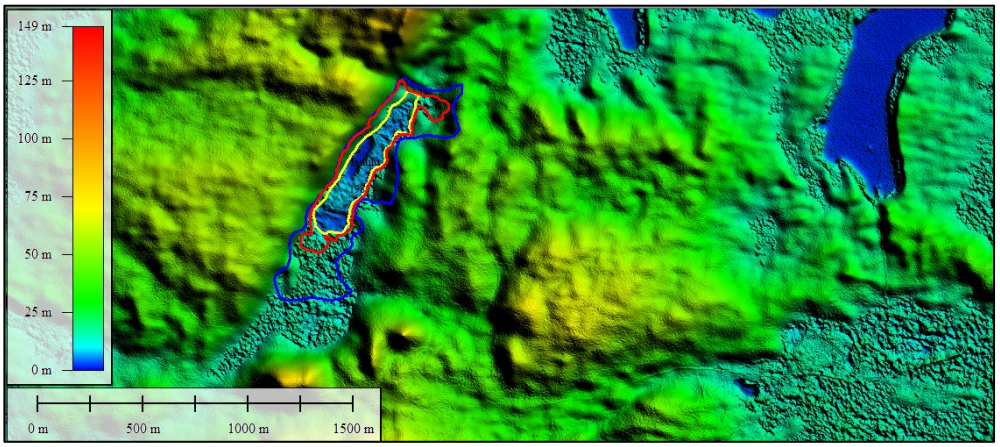

Fig. 5. Bathymetry and topography of Lake Ledulu (1985-2022).

4.4. Profile test of bathymetry and topography

The profile tests carried out consisted of cross-section profile and longitudinal profile tests.

Cross-section profile

The cross-section profile is generated in the west-east direction. The results of the cross-section profile can be seen in **figure 6**. The red line (wet season) is above the yellow line (dry season). This condition means that the water level in the wet season is higher than the water level in the dry season. The difference in water level has an impact on the depth of the lake. The depth of the lake affects the volume of the lake. The volume of the lake in the wet season is greater than the volume of the lake in the dry season.

During the dry season, the water level of Lake Ledulu is around 13 m, while during the wet season, the water level of Lake Ledulu is around 15.5 m. Based on this cross-section profile, the north and west sides of the lake are bordered by steep cliffs of hills. On the north side, it is passed by a sub-fault that divides and limits Lake Ledulu with the hills on the north side bordering the sea. The west side of the lake is hilly with dense vegetation. The hills on the west side are dominated by ocean bedrock. The eastern part of the lake is bounded by hills with a gentler slope. The vegetation on the east side is less dense and dominated by karst rocks.

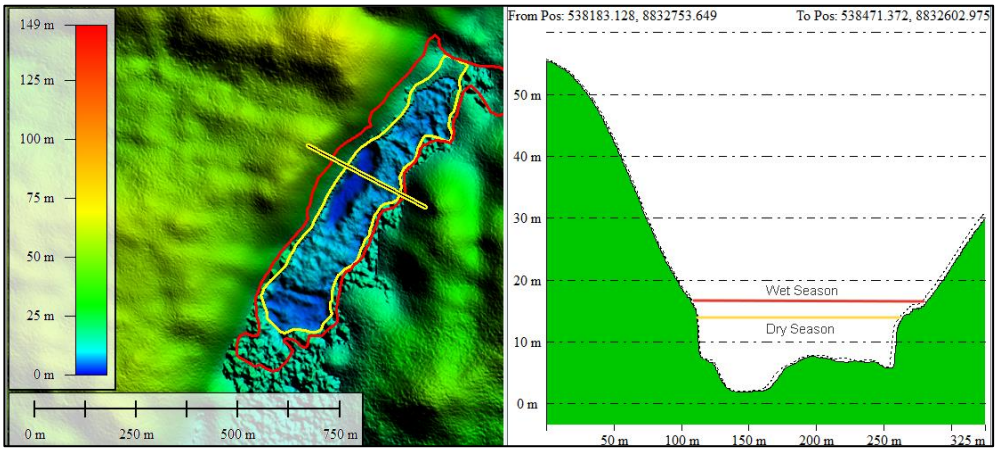

Fig. 6. The cross-section profile of Lake Ledulu in the wet and dry season.

The southern part of the lake is dominated by stretch of swamps filled with mangroves and other vegetation. About 1 km to the south of the lake, hills that have been uplifted and have a height difference of 50-100 m compared to the lakeside are found. The bathymetry of Lake Ledulu from west to east is divided into two characteristics. The western bathymetry is deeper than the eastern bathymetry. The deepest point of the western bathymetry is at an elevation of 4 m in mean sea level (MSL). In the wet season, the maximum depth is 11 m with an average depth of about 5 m. The eastern deepest point is located at an elevation of 8 m MSL or a maximum depth of 7 m with an average depth of 2 m. In dry season conditions, the maximum depth was 8.5 m with an average depth of 2.5 m in the western part of the lake. The eastern region has a maximum depth of 4.5 m with an average depth of 0.5 m. The eastern region is dominated by dense vegetation and grass with a vegetation height of around 1-5 m.

Longitudinal Profile

The next check is carried out by making a longitudinal profile from south to north. The results obtained are the appearances of various bottom topography. Two locations have deeper basins compared to other areas. The first basin is located in the south part of the lake, while the second basin is located in the middle of the lake.

The first basin area in the wet season, the deepest point is located at an elevation of 4.5 m or a depth of 11 m with an average depth of 6 m. The second basin area has the deepest point at an elevation of 3 m or a depth of 12.5 m with an average of 7.5 m. In dry season conditions, the first basin area has a depth of 8.5 m with an average depth of 3.5 m.

The second basin area has a depth of 10 m with an average of 5 m. Based on the appearance of the bathymetry of Lake Ledulu, the complex dynamics of tectonic movements can be seen. The dynamics of the tectonic movement are in the form of fault movements in the north and west of the lake which form steep cliffs. In addition, three sub-fault movements divide the lake, causing two areas that are squeezed and not completely uplifted. These two areas are the areas with maximum depth which are in the south and center of Lake Ledulu. The complex dynamics of tectonic movement with the vertical direction is one of the signs that high vertical deformation has occurred. These conditions support the results of previous studies regarding the vertical deformation value of Rote Island of 13-25 cm/year. If this high vertical deformation is constant in the future, then the potential for Lake Ledulu to become land becomes even greater. **Figure 7** is the longitudinal profile of Lake Ledulu in the wet and dry seasons.

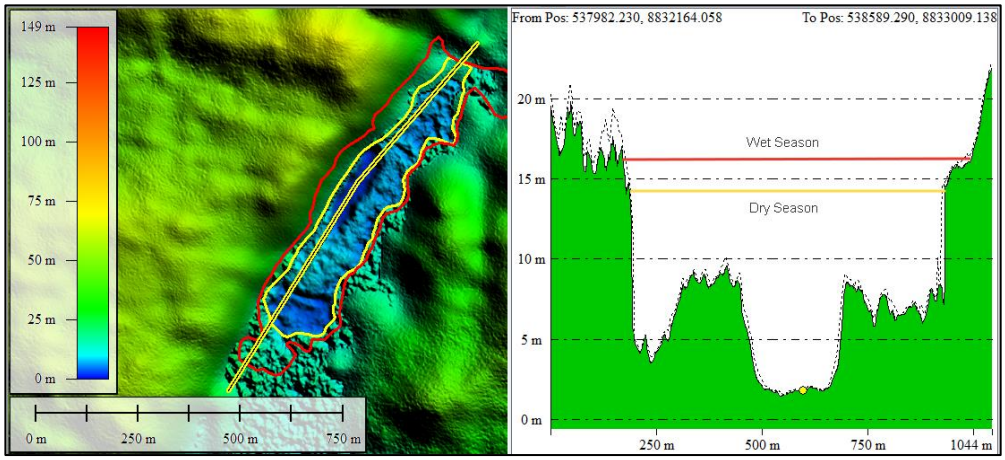

Fig. 7. The longitudinal profile of Lake Ledulu in the wet and dry seasons.

4.5. Vertical accuracy assessment of Lake Ledulu's bathymetry and topography (DTM $_{(2022)}$)

The vertical accuracy test was carried out on DTM $_{(2022)}$. The accuracy test was in the form of a height difference test and a vertical accuracy test. Tests were carried out using 30 points measured in the field with Global Navigation Satellite System (GNSS) with sonar depth measurements and water leveling. In the height difference test, 30 points are made into polygons and the difference in height between the points is added up.

The difference in elevation between these points refers to MSL, whereas all points in the elevation model refer to a specific datum reference plane. The results obtained in the height difference test in this study were a total height difference of ~ 0 m. The DTM $_{(2022)}$ has height relative to the datum due to the points tested (closed polygon) having minimum height difference (close to zero). This condition eliminates any remaining systematic errors in the DTM $_{(2022)}$. The vertical accuracy test was carried out by comparing the orthometric height of the DTM $_{(2022)}$ with the orthometric height of field measurements, see **figure 8**. **Table 1** is the result of the vertical accuracy test of DTM $_{(2022)}$. After checking the difference in height for each point, then check the accuracy of the difference in height at the 95% confidence level according to equation (6). The DTM used includes the detail category (spatial resolution 1 m). The results obtained are a vertical accuracy value of +61.54 cm or <1 m. This DTM can be used for 1:5000 – 1:10000 scale mapping.

Table 1.

The vertical accuracy test of DTM (2022).

No	Longitude	Latitude	H_{data} DTM(m)	Height Difference (m)	H_{check} Ground (m)	$(H_{data} - H_{check})^2$ (m)
1	123.348,449,709	-10.562,885,753	5.2603		5.3000	0.0016
2	123.348,985,702	-10.562,935,934	3.7694	-1.4909	3.8000	0.0009
3	123.348,245,522	-10.562,634,843	5.1122	1.3428	5.2000	0.0077
4	123.348,381,647	-10.562,275,205	5.3269	0.2147	5.4000	0.0053
5	123.348,602,850	-10.562,475,933	4.5548	-0.7721	4.5000	0.0030
6	123.348,883,608	-10.562,584,661	4.4857	-0.0691	4.6000	0.0131
7	123.349,206,906	-10.562,609,752	3.8453	-0.6404	3.8000	0.0021
8	123.349,385,570	-10.562,793,752	3.4687	-0.3766	3.3000	0.0285
9	123.349,412,039	-10.562,399,731	4.6145	1.1458	4.8000	0.0344
10	123.348,757,882	-10.562,790,035	4.4663	-0.1482	4.7000	0.0546
11	123.349,185,163	-10.563,091,127	4.9151	0.4488	5.2000	0.0812
12	123.349,480,101	-10.560,845,944	5.4670	0.5519	5.2000	0.0713
13	123.349,710,758	-10.560,548,568	2.4018	-3.0652	2.4000	0.0000
14	123.349,657,820	-10.560,344,121	2.1233	-0.2785	2.3000	0.0312
15	123.349,907,383	-10.560,280,929	2.4936	0.3703	2.9000	0.1652
16	123.349,888,477	-10.560,039,310	1.7909	-0.7027	1.5000	0.0846
17	123.350,172,071	-10.559,964,966	2.0953	0.3044	2.3000	0.0419
18	123.350,122,914	-10.559,701,044	2.0567	-0.0386	2.2000	0.0205
19	123.350,429,196	-10.559,615,548	3.0569	1.0002	3.8000	0.5522
20	123.350,240,133	-10.559,388,797	2.3891	-0.6678	2.5000	0.0123
21	123.350,485,915	-10.559,199,219	3.3532	0.9641	3.6000	0.0609
22	123.351,383,963	-10.558,760,586	6.0781	2.7249	6.4000	0.1036
23	123.351,607,057	-10.558,552,422	6.3215	0.2434	6.1000	0.0491
24	123.352,117,526	-10.557,545,051	8.2687	1.9472	8.7000	0.1860
25	123.352,257,432	-10.557,284,843	16.0103	7.7416	16.5000	0.2398
26	123.352,756,558	-10.557,630,547	15.5275	-0.4828	15.7000	0.0298
27	123.353,111,996	-10.557,593,375	15.0473	-0.4802	15.8000	0.5666
28	123.353,081,746	-10.558,002,271	16.4595	1.4122	16.1000	0.1292
29	123.350,374,368	-10.560,697,256	4.4982	-11.9613	4.1000	0.1586
30	123.348,169,897	-10.563,239,814	12.0269	7.5287	12.5000	0.2238
1	123.348,449,709	-10.562,885,753	5.2603	-6.7666		
Height Different Test				0.0000	Total $(H_{data} - H_{check})^2$	2.9574
RMSE(z) (Topography) = 0.4452 m; RMSE(z) (Bathymetry) = 0.2714 m RMSE(z) (Topography and Bathymetry) = 0.3140 m						
Vertical Accuracy (Topography) = 0.872551793 m; Vertical Accuracy (Bathymetry) = 0.32012182 m Vertical Accuracy Test (Topography and Bathymetry) = 0.61538516 m						
Vertical Accuracy Test (Topography and Bathymetry) = ± 61.54 cm						

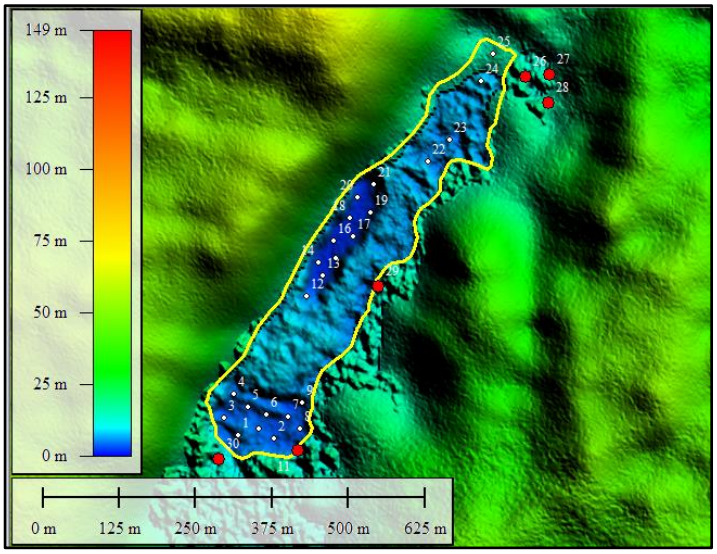

Fig. 8. The 30 measurement points in the field. Red dots were located in topography (outside the Lake Ledulu) and the white dots were located inside of Lake Ledulu. The yellow line was Lake Ledulu shoreline in dry season 2022. We measure all of the points in September-October 2022 (dry season).

6. CONCLUSIONS

The latest bathymetry and topography in Lake Ledulu can be extracted by using modeling with multi-source geospatial data. They include PlanetScope, Sentinel-1, Landsat images, and in-situ field data. The DTM $_{(2022)}$ Lake Ledulu has a vertical accuracy of 61.54 cm or according to 1:5000 – 1:10000 scale mapping with confidence level (95 %) according to the ASPRS 2014. DTM $_{(2022)}$ was used to determine the dynamics of the volume of Lake Ledulu and its changing from 1985 to 2022. In 2022 (dry season) Lake Ledulu has a surface area of 0.0946 km^2 and a volume of 701,688.45 m^3. The total length/perimeter of Lake Ledulu was 1.868 km. The surface area of Lake Ledulu in the wet season (2022) was 0.1555 km^2 with a volume of 1,116,525.9 m^3. The total perimeter was 2.612 km.

The surface area of Lake Ledulu in 1985 was 0.3079 km^2 with a perimeter of 3.477 km. The volume of Lake Ledulu in 1985 was 4,772,567.2 m^3. The change in the surface area of Lake Ledulu from 1985-2022 was 0.1525 km^2. Changes in the surface area of Lake Ledulu experienced a decrease of 49.53%. The volume of Lake Ledulu between 1985-2022 was 3,656,041.3 m^3 (decrease of 75.61%). The changing of Lake Ledulu perimeter in 1985-2022 was 0.862 km. Changes in the perimeter of Lake Ledulu experienced a shrinkage of 24.79%.

ACKNOWLEDGEMENTS

We would like to thank the Indonesian National Research and Innovation Agency (BRIN), Ministry for Environment and Forestry (KLHK), Nusa Cendana University, and Matara Family for supporting this research. There is no external and internal funding for this publication. All authors are the main contributors to this paper. The authors reported no potential conflicts of interest.

REFERENCES

Alpers, W., & Hennings, I. (1984). A theory of the imaging mechanism of underwater bottom topography by real and synthetic aperture radar. *Journal of Geophysical Research: Oceans*, *89*, 0529–10546. https://doi.org/10.1029/JC089iC06p10529

ASPRS Accuracy Standards for Digital Geospatial Data, The American Society for Photogrammetry and Remote Sensing (2014). https://doi.org/10.1016/S0033-3506(98)80082-6

Baek, J., & Choi, Y. (2017). A new algorithm to find raster-based least-cost paths using cut and fill operations. *International Journal of Geographical Information Science*, *31*(11), 2234–2254. https://doi.org/10.1080/13658816.2017.1356463

Bignone, F., Umakawa, H., Sensing, R., Centre, S., & Aperture, L. S. (2008). Assessment of Alos Prism Digital Elevation Model Extraction Over Japan. *The International Archives of the Photogrammetry, Remote Sensing and Spatial Information Sciences*, *XXXVII. Pa*, 1135–1138.

Costantini, M. (1998). A novel phase unwrapping method based on network programming. *IEEE Transactions on Geoscience and Remote Sensing*, *36*(3), 813–821. https://doi.org/10.1109/36.673674

Devanthéry, N., Crosetto, M., Cuevas-González, M., Monserrat, O., Barra, A., & Crippa, B. (2016). Deformation Monitoring Using Persistent Scatterer Interferometry and Sentinel-1 SAR Data. *Procedia Computer Science*, *100*, 1121–1126. https://doi.org/10.1016/j.procs.2016.09.263

Fukuda, T., Tokuhara, T., & Yabuki, N. (2016). A dynamic physical model based on a 3D digital model for architectural rapid prototyping. *Automation in Construction*, *72*, 9–17. https://doi.org/10.1016/j.autcon.2016.07.002

Ghilani, C. D., & Wolf, P. R. (2006). *Adjustment Computations Spatial Data Analyses 4th Edition*. https://doi.org/10.1038/ni1566

Hall, R. (2011). Australia-SE Asia collision: Plate tectonics and crustal flow. *Geological Society Special Publication*, *355*, 75–109. https://doi.org/10.1144/SP355.5

Hambali, A., Santoso, A. I., Setiawan, K. T., Julzarika, A., Setiyadi, J., & K, E. S. (2021). Utilization of PlanetScope Image For Batimetry Estimation, Case Study In Shallow Sea Waters Of Karimunjawa Island, Jepara, Central Java. *Hidropilar*, *7*(1), 23–30.

Herrera, G., Gutiérrez, F., García-davalillo, J. C., Guerrero, J., Notti, D., & Galve, J. P. (2013). Remote Sensing of Environment Multi-sensor advanced DInSAR monitoring of very slow landslides : The Tena Valley case study (Central Spanish Pyrenees). *Remote Sensing of Environment*, *128*, 31–43. https://doi.org/10.1016/j.rse.2012.09.020

Hoja, D., & D'Angelo, P. (2010). Analysis of DEM combination methods using high resolution optical stereo imagery and interferometric SAR data. *International Archives of the Photogrammetry, Remote Sensing and Spatial Information Science,Volume XXXVIII,Part 1*, 02–05. https://doi.org/10.1007/978-3-319-59489-7

IHB. (2006). *Technical Aspect of the Law of the Sea (TALOS)* (I. UNESCO, IOC, IHO (ed.)). International Hydrographic Bureau (IHB). United Nation.

Inglada, J., & Garello, R. (2002). On rewriting the imaging mechanism of underwater bottom topography by synthetic aperture radar as a volterra series expansion. *IEEE Journal of Oceanic Engineering*, *27*, 665–674. https://doi.org/10.1109/JOE.2002.1040949

Jenson, S. K., & Domingue, J. O. (1988). Extracting topographic structure from digital elevation data for geographic information-system analysis. *Photogrammetric Engineering and Remote Sensing*, *54*(11), 1593–1600. http://pubs.er.usgs.gov/publication/70142175

Julzarika, A., & Harintaka. (2020). Utilization of DSM and DTM for Spatial Information in Lake Border. *IOP Conference Series: Earth and Environmental Science*, *535*(1). https://doi.org/10.1088/1755-1315/535/1/012034

Julzarika, A., Laksono, D. P., Kayat, Subehi, L., Dewi, E. K., Sofiyuddin, H. A., Nugraha, M. F. I., Anggraini, N., Setianto, A., Janwes, & Yudhatama, D. (2020). Realizing the Dead Sea Lakes Region in Rote Islands to be a geopark using multidisciplinary spatial information approach. *IOP Conference Series: Earth and Environmental Science*, *535*(1). https://doi.org/10.1088/1755-1315/535/1/012033

Julzarika, Atriyon. (2015). Height Model Integration Using ALOS PALSAR, X SAR, SRTM C, and IceSAT/GLAS. *International Journal of Remote Sensing and Earth Sciences*, *12*(2), 107–116. https://doi.org/nrrheum.2016.1 [pii]\r10.1038/nrrheum.2016.1 [doi]

Julzarika, Atriyon. (2021). *The Updated DTM Model using ALOS PALSAR/PALSAR-2 and Sentinel-1 Imageries for Dynamic Topography*. Universitas Gadjah Mada.

Julzarika, Atriyon, Aditya, T., Subaryono, Harintaka, Dewi, R. D., & Subehi, L. (2021). Integration of the latest Digital Terrain Model (DTM) with Synthetic Aperture Radar (SAR) Bathymetry. *J. Degrade. Min. Land Manage*, *8*(3), 2502–2458. https://doi.org/10.15243/jdmlm

Julzarika, Atriyon, Aditya, T., Subaryono, S., & Harintaka, H. (2021). The latest dtm using insar for dynamics detection of semangko fault-indonesia. *Geodesy and Cartography (Vilnius)*, *47*(3), 118–130. https://doi.org/10.3846/gac.2021.12621

Julzarika, Atriyon, Aditya, T., Subaryono, S., & Harintaka, H. (2022). Dynamics Topography Monitoring in Peatland Using the Latest Digital Terrain Model. *Journal of Applied Engineering Science*, *20*(1), 246–253. https://doi.org/10.5937/jaes0-31522

Julzarika, Atriyon, Anggraini, N., Kayat, K., & Pertiwi, M. (2018). Land changes detection on Rote Island using harmonic modelling method. *J. Degrade. Min. Land Manage*, *5*(53), 2502–2458. https://doi.org/10.15243/jdmlm

Julzarika, Atriyon, & Djurdjani, D. (2018). DEM classifications: opportunities and potential of its applications. *J. Degrade. Min. Land Manage*, *5*(53). https://doi.org/10.15243/jdmlm

Julzarika, Atriyon, & Harintaka. (2019). *UTILIZATION OF SENTINEL SATELLITE FOR VERTICAL DEFORMATION MONITORING IN SEMANGKO FAULT-INDONESIA*. *Acrs*, 1–7.

Julzarika, Atriyon, & Harintaka. (2020). Indonesian DEMNAS: DSM or DTM? *2019 IEEE Asia-Pacific Conference on Geoscience, Electronics and Remote Sensing Technology (AGERS)*, 31–36. https://doi.org/10.1109/AGERS48446.2019.9034351

Julzarika, Atriyon, Laksono, D. P., Subehi, L., Dewi, E. K., Kayat, K., Sofiyuddin, H. A., & Nugraha, M. F. I. (2018). Comprehensive integration system of saltwater environment on Rote Island using a multidisciplinary approach. *J. Degrade. Min. Land Manage*, *5*(53), 2502–2458. https://doi.org/10.15243/jdmlm

Kubla. (2019). *How Accurate is the Grid Method For Calculating Earthworks Cut & Fill Volumes?* https://www.kublasoftware.com/grid-method-accuracy/

Laksono, D., Julzarika, A., Subehi, L., Sofiyuddin, H. A., Dewi, E. K., N, M. F. I., Pekerjaan, K., Rakyat, P., & Kelautan, K. (2019). Expedition Oe : A Visual- storytelling map on Rote Island ' s Lakes. *Journal of Geospatial Information Science and Engineering*, *1*(2), 87–93.

Li, Z., Zhu, Q., & Gold, C. (2004). Digital terrain modeling: Principles and methodology. In *Digital Terrain Modeling: Principles and Methodology*. https://doi.org/10.1201/9780203357132

Malaspinas, A. S., Westaway, M. C., Muller, C., Sousa, V. C., Lao, O., Alves, I., Bergström, A., Athanasiadis, G., Cheng, J. Y., Crawford, J. E., Heupink, T. H., MacHoldt, E., Peischl, S., Rasmussen, S., Schiffels, S., Subramanian, S., Wright, J. L., Albrechtsen, A., Barbieri, C., … Willerslev, E. (2016). A genomic history of Aboriginal Australia. *Nature*, *538*(7624), 207–214. https://doi.org/10.1038/nature18299

Nasir, S., Iqbal, I. A., Ali, Z., & Shahzad, A. (2015). Accuracy assessment of digital elevation model generated from pleiades tri stereo-pair. *RAST 2015 - Proceedings of 7th International Conference on Recent Advances in Space Technologies*, 193–197. https://doi.org/10.1109/RAST.2015.7208340

Ndao, P. K. R. (2021). *Profil Daerah Kabupaten Rote Ndao*. Pemda Kabupaten Rote Ndao. https://rotendaokab.go.id/profil-daerah

Nico, G., Leva, D., Fortuny-Guasch, J., Tarchi, D., & Antonello, G. (2005). Generation of digital terrain models with a ground-based SAR system. *IEEE Transactions on Geoscience and Remote Sensing*, *43*(1), 45–49. https://doi.org/10.1109/TGRS.2004.838354

Pleskachevsky, A., Lehner, S., Heege, T., & Mott, C. (2011). Synergy and fusion of optical and synthetic aperture radar satellite data for underwater topography estimation in coastal areas. *Ocean Dynamic*, *61*(12), 2099–2120. https://doi.org/10.1007/s102-011-0460-1

Rucci, A., Ferretti, A., Monti Guarnieri, A., & Rocca, F. (2012). Sentinel 1 SAR interferometry applications: The outlook for sub millimeter measurements. *Remote Sensing of Environment*, *120*, 156–163. https://doi.org/10.1016/j.rse.2011.09.030

Ruzgiene, B., Berteška, T., Gečyte, S., Jakubauskiene, E., & Aksamitauskas, V. Č. (2015). The surface modelling based on UAV Photogrammetry and qualitative estimation. *Measurement: Journal of the International Measurement Confederation*, *73*, 619–627. https://doi.org/10.1016/j.measurement.2015.04.018

Samboko, H. T., Abas, I., Luxemburg, W. M. J., Savenije, H. H. G., Makurira, H., Banda, K., & Winsemius, H. C. (2020). Evaluation and improvement of remote sensing-based methods for river flow management. *Physics and Chemistry of the Earth*, *117*, 102839. https://doi.org/10.1016/j.pce.2020.102839

Sesama, A. S., Setiawan, K. T., & Julzarika, A. (2021). Bathymetric Extraction Using Planetscope Imagery (Case Study: Kemujan Island, Central Java). *International Journal of Remote Sensing and Earth Sciences (IJReSES)*, *17*(2), 209. https://doi.org/10.30536/j.ijreses.2020.v17.a3445

Setiawan, K. T., Suwargana, N., Br. Ginting, D. N., Manessa, M. D. M., Anggraini, N., Adawiah, S. W., Julzarika, A., Surahman, S., Rosid, S., & Supardjo, A. H. (2019). Bathymetry Extraction From Spot 7 Satellite Imagery Using Random Forest Methods. *International Journal of Remote Sensing and Earth Sciences (IJReSES)*, *16*(1), 23. https://doi.org/10.30536/j.ijreses.2019.v16.a3085

Simons, M., & Rosen, P. A. (2015). Interferometric Synthetic Aperture Radar Geodesy. In *Treatise on Geophysics: Second Edition* (Vol. 3). Elsevier B.V. https://doi.org/10.1016/B978-0-444-53802-4.00061-0

Suhadha, A. G., & Julzarika, A. (2020). Integration of Remote Sensing and Geographic Information System for Mapping Potential Tsunami Inundation. *Proceeding - AGERS 2020: IEEE Asia-Pacific Conference on Geoscience, Electronics and Remote Sensing Technology: Understanding the Interaction of Land, Ocean and Atmosphere: Disaster Mitigation and Regional Resillience*, *December*, 163–167. https://doi.org/10.1109/AGERS51788.2020.9452767

Suhadha, A. G., & Julzarika, A. (2022). Dynamic Displacement using DInSAR of Sentinel-1 in Sunda Strait. *Trends in Sciences*, *19*(13), 4623. https://doi.org/10.48048/tis.2022.4623

Suhadha, A. G., Julzarika, A., Ardha, M., & Chusnayah, F. (2021). Monitoring Vertical Deformations of the Coastal City of Palu after Earthquake 2018 Using Parallel-SBAS. *Proceedings - 2021 7th Asia-Pacific Conference on Synthetic Aperture Radar, APSAR 2021*, *March*. https://doi.org/10.1109/APSAR52370.2021.9688380

Uysal, M., Toprak, A. S., & Polat, N. (2015). DEM generation with UAV Photogrammetry and accuracy analysis in Sahitler hill. *Measurement: Journal of the International Measurement Confederation*, *73*. https://doi.org/10.1016/j.measurement.2015.06.010

Wilson, J. (2012). Digital terrain model. *Regional Assessment of Global Change Impacts: The Project GLOWA-Danube*, *137*(1), 69–74. https://doi.org/10.1007/978-3-319-16751-0_7

Wulandari, S. A., & Wicaksono, P. (2021). Bathymetry mapping using PlanetScope imagery on Kemujan Island, Karimunjawa, Indonesia. *The International Conference on Smart and Innovative Agriculture (IOP Conf. Series: Earth and Environmental Science 686 (2021) 012032)*, 1–11. https://doi.org/10.1088/1755-1315/686/1/012032